Korean J. Chem. Eng., **30**(10), 1836-1842 (2013)
DOI: 10.1007/s11814-013-0124-6

Optimization of temperature swing strategy for selective cooling crystallization of α-form L-glutamic acid crystals

Seungjong Yeom, Huichan Yun, and Dae Ryook Yang†

Department of Chemical and Biological Engineering, Korea University,
Anam-dong 5-Ga, Seongbuk-gu, Seoul 136-701, Korea
(*Received 31 May 2013 • accepted 9 July 2013*)

Abstract−L-glutamic acid can be crystallized as metastable α-form and stable β-form crystal. The α-form is desired because of its prismatic shape. Production of α-form of L-glutamic acid by cooling crystallization is not well-defined and α-form solid is commercially not available. In this study, an optimal cooling strategy to selectively produce large and narrowly distributed α-crystals is found by modeling and optimizing the crystallization and polymorphic transformation of L-glutamic acid. The optimal temperature profile is found to be cooling-heating-cooling concept where short nucleation period is followed by growth period in metastable zone. The obtained α-form of L-glutamic acid by optimal strategy had improved mean size, distribution, and purity compared to constant cooling.

Key words: Cooling Crystallization, Population Balance Model, Polymorphic Transformation, L-Glutamic Acid, Optimization

INTRODUCTION

Many organic crystals have two or more polymorphic forms and each form has its own properties such as crystal habit, solubility, bioavailability, and so on. In solution crystallization, less stable form of crystals can be transformed into more stable form in the magma and this phenomenon is called solvent-mediated polymorphic transformation. The transformation occurs owing to different thermodynamic stability of each polymorph in a certain operating condition. Because the purity, ease of industrial handling, drug efficiency and other factors of product quality are closely related to the concentration of polymorphs, many research groups have studied the monitoring and modeling of polymorphic transformation [1-4].

L-glutamic acid (LGA) has two polymorphs, metastable α-form and stable β-form. The α-form is a prismatic crystal and β-form is a needle-like crystal. The needle-like crystal is easy to break, so α-form is preferred due to its shape [5]. However, metastable α-form is not commercially available [6]. The α-form can be produced by either rapid cooling [7] or acidification of monosodium L-glutamate (MSG) [6-11].

Rapid cooling for production of α-form has been reported by several researchers. Kitamura et al. obtained α-form by rapid cooling of the solution saturated at 70 °C [7]. To obtain pure α-form, Mo et al. prepared solution at 80 °C, and cooled it to 20 °C rapidly [12]. De Anda et al. produced α-form by constant cooling of the solution from 95 to 15 °C. They reported that with cooling rates of 0.25 and 0.5 °C/min, crystallized α-form was gradually transformed into β-form, but with 1 °C/min, there was no transformation to β-form [13]. As seen in these reports, strategies for producing α-form LGA by cooling crystallization have been vague and not well-defined.

Efforts to obtain pure α-form LGA had been made by Kee et al. using feedback control. They adjusted solute concentration so as for supersaturation level to remain in metastable zone and close to the metastable limit [14].

The metastable limit is where spontaneous primary nucleation occurs when the solute concentration exceeds that limit. From the viewpoint of crystal growth, the necessity to inhibit excessive nucleation gives rise to the importance of metastable limit. Despite the significance of metastable limit, it is very difficult to measure exactly and also has not been fully understood theoretically. Yang et al. suggested dynamic metastable limit, which is not a fixed curve but may be influenced by cooling rate, so can only be determined by solving differential equation with respect to time [15,16].

Mathematical modeling of processes involving particles such as crystallization often requires population balance equations (PBE). For example, crystallization of drug ingredient [17], enantiomers [18], and protein [19] could be analyzed by using PBE. Ma et al. identified morphological population balance model expressing crystal growth of LGA [20,21]. Population balance equation is a partial differential equation with respect to two independent variables and this leads to difficulty in solving the equation. The PBE in crystallization models have been solved and utilized by many researchers who study crystallization processes, and a number of numerical skills to obtain solutions of PBE have been introduced. Kumar et al. suggested a moving pivot technique in solving PBE for accurate prediction of number density of large particles [22,23]. Gerstlauer et al. proposed a population balance model that considers two particle properties, crystal length and also internal lattice strain of crystals [24]. The PBE solutions describing reversible growth and dissolution were discussed by McCoy [25,26] and Madras [27]. Puel et al. applied multidimensional PBE to simulation of crystallization processes [28,29] and Gunawan et al. introduced high resolution algorithms for multi-dimensional PBE [30]. Hu et al. came up with a new numerical method which enables solving PBE as discretized algebraic equations [31,32]. Févotte et al. described adsorption of impurities

†To whom correspondence should be addressed.
E-mail: dryang@korea.ac.kr

during crystallization by using a method of characteristics for solving PBE [33]. Silva et al. compared quadrature-based methods [34] and Samad et al. generalized and organized various kinds of multi-dimensional models for cooling crystallization [35].

Mathematical models of solvent-mediated polymorphic transformation of LGA have been developed for a few years. Schöll et al. introduced kinetic model including birth, growth and dissolution of both forms of crystals, and estimated parameters of the model [36]. Hermanto et al. suggested parameter estimation by Bayesian inference in LGA transformation modeling [37]. Qamar et al. devised an efficient numerical solution of crystallization model for LGA polymorphs. They employed method of characteristics and Duhamel's principle instead of Laplace transform. Their calculation result was validated by comparing with the result of finite volume scheme of Koren [38].

In cooling crystallization, addition of a heating step has been considered as a simple strategy to enhance crystal growth and size distribution. To obtain large crystals, solute has to be spent in growth of large particles rather than tiny particles. The role of heating step is often that of dissolving fine particles so that only large particles grow [39].

In this study, the model for polymorphic transformation of LGA was established for simulation and optimization of cooling crystallization of LGA. In order not to generate excessive amount of fine particles, the heating step in cooling profile is introduced and it shifts the solute concentration into metastable zone to facilitate growth of α-form LGA instead of undesired nucleation of fine particles. The cooling trajectory was optimized to produce large and sharply distributed pure α-form LGA crystals.

MODEL

The model of this study is comprised of kinetics, population balance and mass balance equations. The equations are discretized with respect to time and characteristic length and then solved by using MATLAB. The solubility data for LGA from Hermanto et al. was used for supersaturation calculation. Solubility of α- and β-crystals from 25 to 60 °C was measured using IR and expressed as a quadratic equations [37].

$$C^*_\alpha = a_{\alpha 1}T^2 + a_{\alpha 2}T + a_{\alpha 3} \tag{1}$$

$$C^*_\beta = a_{\beta 1}T^2 + a_{\beta 2}T + a_{\beta 3} \tag{2}$$

The supersaturation is defined as current solute concentration divided by saturated solute concentration.

$$S_\alpha = C/C^*_\alpha \tag{3}$$

$$S_\beta = C/C^*_\beta \tag{4}$$

The metastable limit data of Kee et al. was used in calculation of nucleation kinetics. A few data points are obtained by detecting sharp increase of FBRM counts while gradually decreasing the temperature of under-saturated LGA solution [14]. For the simplicity of the model, the data points are fitted into exponential curve instead of formulating dynamic equation for metastable zone width.

$$C_{met} = z_0 \exp(z_1 T) \tag{5}$$

Equations and parameters for crystallization kinetics are excerpted from Schöll et al. Nucleation of α- and β-LGA is formulated as below [36].

$$B_\alpha = k_{n\alpha} S_\alpha^{7/3} \exp(-K_{n\alpha}/\ln^2 S_\alpha) \tag{6}$$

$$B_\beta = k_{n\beta} S_\beta^{7/3} \exp(-K_{n\beta}/\ln^2 S_\beta) + k_{s\beta} m_{2\alpha} \exp(-K_{s\beta}/\ln S_\beta) \tag{7}$$

The second term in the equation of β nucleation denotes birth of β-crystal on the surface of α-crystal. The $m_{2\alpha}$ is the second moment of α-form, which represents total surface area of α-crystals.

$$m_{2\alpha} = \sum_i L^2_{\alpha,i} n_{\alpha,i} (\Delta L)_{\alpha,i} \tag{8}$$

$L_{\alpha,i}$ is the characteristic length (size) and $n_{\alpha,i}$ is number density of i-th node of α-crystal size. Growth rates of α- and β-crystal are functions of supersaturation ratio [36].

$$G_\alpha = k_{g\alpha}(S_\alpha - 1)^{5/6} \exp(-K_{g\alpha}/(S_\alpha - 1)) \tag{9}$$

$$G_\beta = k_{g\beta}(S_\beta - 1)^{5/6} \exp(-K_{g\beta}/(S_\beta - 1)) \tag{10}$$

It is assumed that the dissolution rate is simply proportional to the supersaturation ratio.

$$D_\alpha = k_{d\alpha}(1 - S_\alpha) \tag{11}$$

Coefficient $k_{d\alpha}$ is related to diffusivity (D), average power input ($\bar{\varepsilon}$), kinematic viscosity (ν), and Schmidt number (Sc) [36].

$$k_{d\alpha} = \frac{D}{L_\alpha}\left(2 + 0.8\left(\frac{\bar{\varepsilon} L_\alpha^4}{\nu^3}\right)^{1/5} Sc^{1/3}\right) \tag{12}$$

The population balance equation below is used to calculate crystal size distribution (CSD).

$$\frac{\partial n_\alpha}{\partial t} + \frac{\partial (G_\alpha n_\alpha)}{\partial L_\alpha} = 0 \tag{13}$$

The partial differential equation above is approximated to the form suggested by Hu et al. [31].

$$n_\alpha(t,i) = \frac{n_\alpha(t-1, i-1)}{1 + \dfrac{\partial G_\alpha}{\partial L_\alpha}(t,i)\Delta t} \tag{14}$$

The CSD of β-crystals can be calculated by same form of approximated population balance equation as that of α-crystals. Mass balances for α and β solid concentration (c_α and c_β) are established.

$$\frac{dc_\alpha}{dt} = 3k_{a\alpha}\rho_\alpha \int_0^\infty (G_\alpha - D_\alpha) n_\alpha L_\alpha^2 dL_\alpha \tag{15}$$

$$\frac{dc_\beta}{dt} = 3k_{a\beta}\rho_\beta \int_0^\infty (G_\beta - D_\beta) n_\beta L_\beta^2 dL_\beta \tag{16}$$

where ρ_α and ρ_β are the densities of α and β particles, respectively. The mean and standard deviation of α crystals ($\bar{L}_\alpha$ and σ_α) are defined for evaluation of CSD.

$$\bar{L}_\alpha = \frac{\sum_i L_{\alpha,i} n_{\alpha,i}}{\sum_i n_{\alpha,i}} \tag{17}$$

$$\sigma_\alpha = \sqrt{\frac{\sum_i (L_{\alpha,i} - \bar{L}_\alpha)^2 n_{\alpha,i}}{\sum_i n_{\alpha,i}}} \tag{18}$$

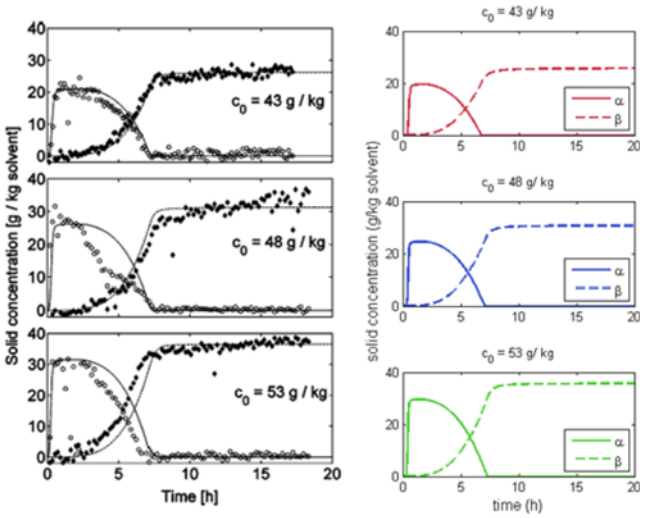

Fig. 1. (a) Solid concentration profiles of Scholl et al. (b) Solid concentration profiles of this study.

RESULTS

1. Model Validation

To validate the established model, crystallization and polymorphic transformation of LGA was simulated with operating condition in Schöll et al. Initial temperature is 80 °C and the solution is constantly cooled to 45 °C at the cooling rate of 1.5 K/min. Three different initial solute concentration conditions were used in simulation. The simulated solid concentration profiles are consistent with those of Schöll et al. as in Fig. 1. The crystal size distribution (CSD) is also compared with each other in Fig. 2. Because y-axis of Fig. 2(a) and that of Fig. 2(b) have different quantity, numerical comparison is not available. However, similar trends in two CSD plots are that crystal size ranges between 10 and 1,000 μm, and the number of β-form crystals of certain size is about five times larger than that of α-form crystals as in the figure.

2. Case Study

To find a strategy better in producing pure and well-grown α-particles than constant cooling strategy, two case studies were done. Using the model developed, two cases of different temperature profiles were simulated. Case 1 is a typical linear cooling crystallization and Case 2 is cooling crystallization where temperature swing is applied. In Case 1, temperature declines from initial temperature 80 to 30 °C in constant cooling rate during 120 minutes. In Case 2, the temperature profile has three regions. Temperature decreases from 80 to 55 °C during first 30 minutes, increases to 60 °C until 60 minutes have elapsed, and then decreases again to 30 °C until 120 minutes is reached. In each region, cooling or heating rate is constant. The simulation results are represented in Fig. 3. In Fig. 3(a), the region between metastable limit and α-solubility is called metastable zone. In the metastable zone, nucleation is inhibited and growth of existing crystals occurs. Solid concentration trajectory of Case 2 goes into metastable zone earlier than that of Case 1. As a result, size distribution of Case 2 is less dispersed and has larger mean crystal size than Case 1 does (Table 1). This shows that the longer the time spent in metastable zone, less nucleation of fine particles occurs and the more growth of larger particles accelerates. To enter metastable zone sooner, first cooling region should be shorter. However, too early heating may end up with substantially insufficient production of α-form crystal nuclei and further cooling after that heating becomes useless. On the other hand, for the growth of α-form, cooling duration after heating should be extended so that the solute concentration level can stay longer in metastable zone. However, long duration in the zone may cause the increase of the amount of undesired β-form. Thus, optimization of temperature profile can provide an appropriate solution for this problem.

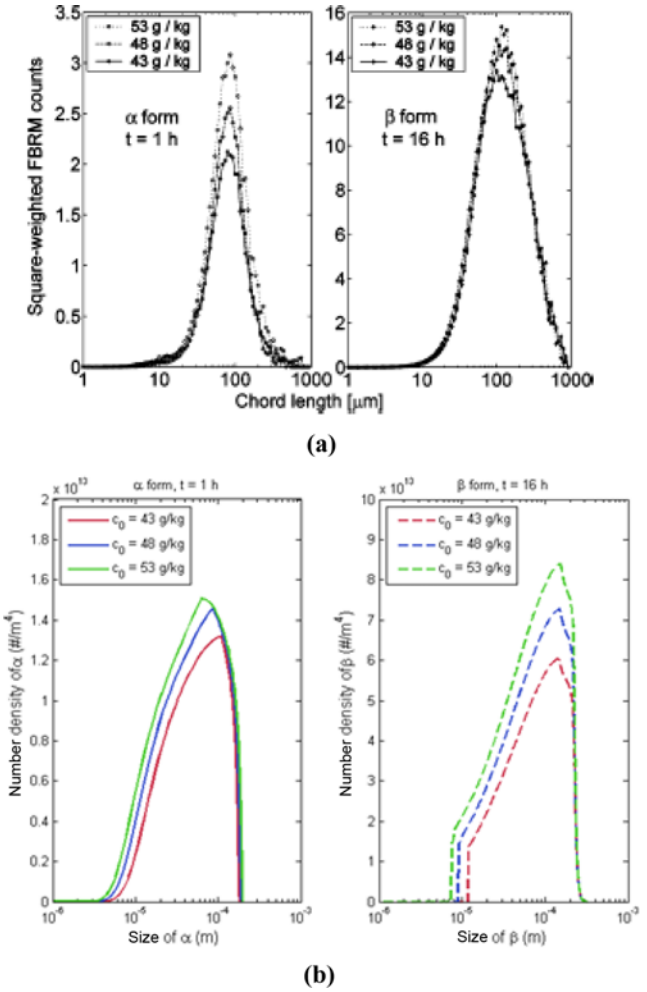

Fig. 2. (a) Size distribution of Scholl et al. (b) Size dis-tribution of this study.

3. Optimization

Based on the case study, cooling strategies composed of initial cooling, heating, and final cooling steps are considered. Initial cooling step induces appropriate nucleation of α-crystals. Heating step pushes the degree of saturation of solution into the metastable zone so that excessive nucleation is prohibited. Final cooling step is programmed to operate within metastable zone where only growth of crystals is allowed without primary nucleation. Temperature in final cooling step is controlled for solute concentration to be in the range of 95-100% of metastable zone width when α-saturation limit is 0% and metastable limit is 100%. The maximum cooling rate is set to 1.50 K/min.

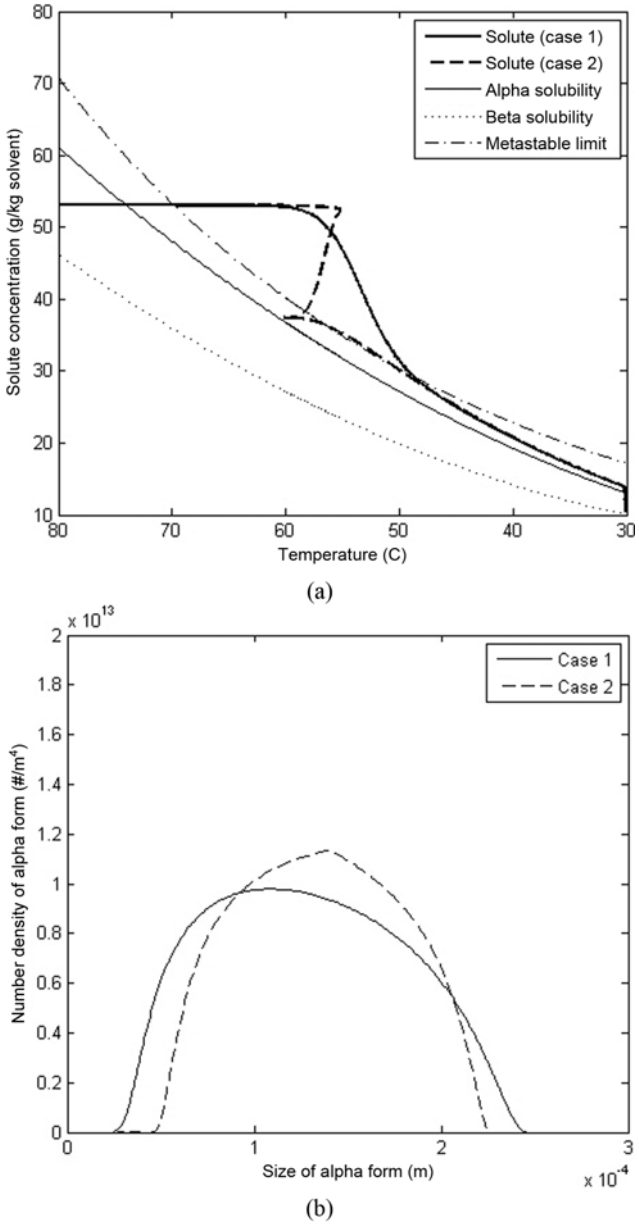

Fig. 3. (a) Solute concentration in two cases with respect to temperature. Solubility curves of α- and β-form and metastable limit are also plotted. (b) Crystal size distribution of α-form in two cases.

Table 1. Simulation results of Case 1 and Case 2.

	Case 1	Case 2
c_α	38.82 g/kg solvent	38.32 g/kg solvent
$\overline{L}_\alpha$	132.19 μm	135.64 μm
σ_α	56.25 μm	47.94 μm

The objective function is formulated to optimize the production of α-LGA by three-step strategy above.

$$\max_{r,T_c} J = w_1 Y_\alpha + w_2 x_\alpha + (w_3 l - w_4 \sigma) \tag{19}$$

where w_1, w_2, w_3 and w_4 are weighting factors, r is the heating rate in heating step and T_c is the temperature where initial cooling ends. The initial cooling rate is set as 1.50 K/min for considering the capacity of cooling equipment. Through studying various cases, the feasible ranges of r and T_c were determined as below.

$$-0.50\ \text{K/min} \le r \le 1.50\ \text{K/min} \tag{20}$$

$$45\ ^\circ\text{C} \le T_c \le 65\ ^\circ\text{C} \tag{21}$$

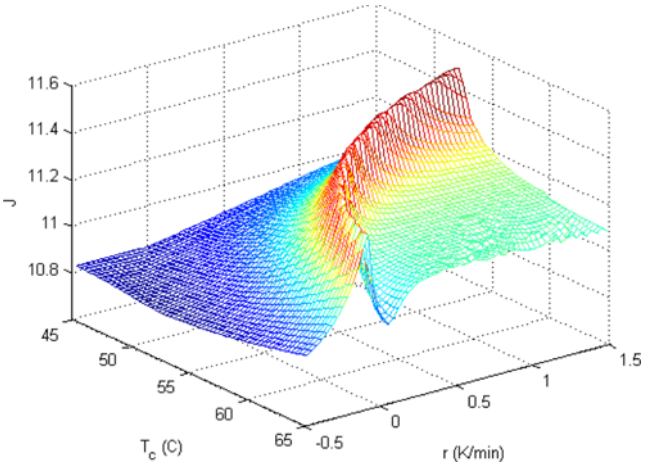

Fig. 4. Objective function depending on variables.

Table 2. Simulation results of optimal and base cases

	Optimal case	Base case
c_α	28.19 g/kg solvent	29.43 g/kg solvent
$\overline{L}_\alpha$	138.17 μm	101.44 μm
σ_α	34.56 μm	56.30 μm
c_β	0.25 g/kg solvent	0.56 g/kg solvent
x_α	99.13%	98.14%

To compare with the base case of constant cooling and holding, final temperature was set to be 45 °C and the duration of operation was fixed as 2 hours. Y_α is the yield of α-L-glutamic acid defined as a ratio between produced α particle concentration and initial solute concentration ($Y_\alpha = c_\alpha/c_0$). Also, x_α is the purity of α-form defined as a mass fraction of α-solid ($x_\alpha = c_\alpha/(c_\alpha + c_\alpha)$), l is the average α-crystal length in microns ($l = \overline{L}_\alpha/10^{-6}$), σ is the standard deviation of α-crystal size distribution in microns ($\sigma = \sigma_\alpha/10^{-6}$).

The objective function values are plotted in Fig. 4. The optimization was conducted by enumeration because of discontinuity of objective function due to the numerical nature related to discretization for time grid width and resolution of temperature control precision. The optimum is obtained when r=1.47 K/min, and T_c=52 °C. The optimal case is compared with base case which is constant cooling from 80 to 45 °C and holding until 2 h. The simulated data of produced solid is tabulated in Table 2. The size, distribution, and purity of α-crystals are all improved by the obtained optimal strategy. When the optimal strategy was applied, the average size of α-crystal became 36% larger, dispersion of α-crystal size became 39% narrower, and the fraction of impurity (β-form) became about half of the base case. In Fig. 5, the optimal and base cases are compared in detail. Temperature profile of optimal case is composed of

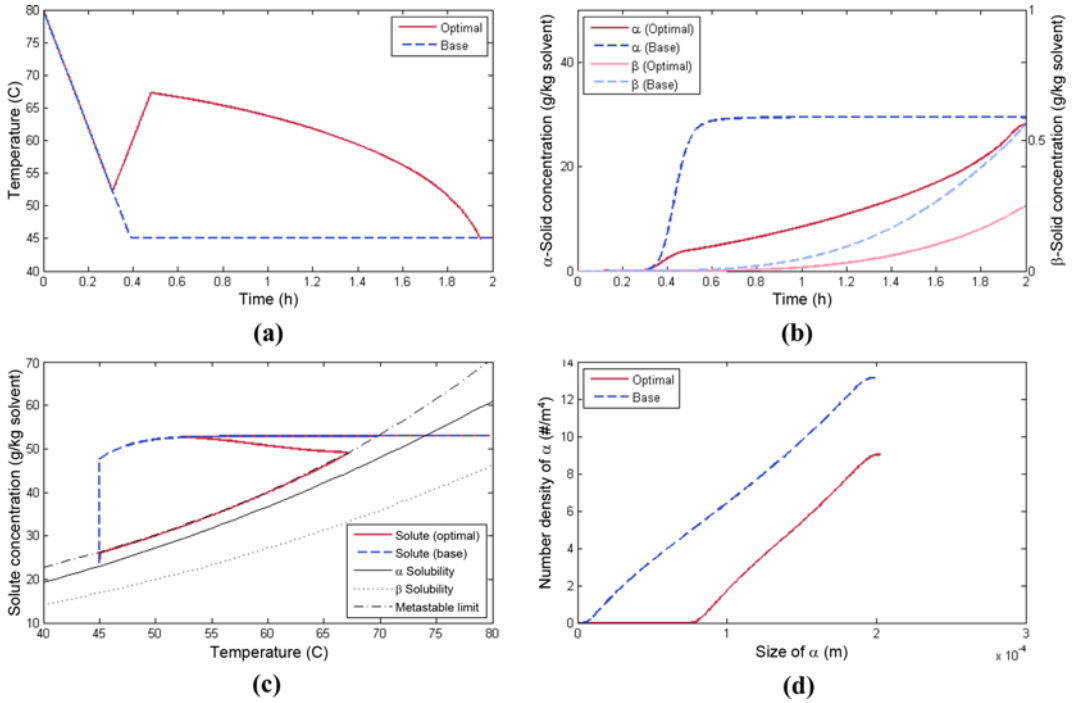

Fig. 5. Simulation results of optimal and base cases (a) temperature profiles (b) solid concentration profiles of poly-morphs (c) solute concentration profiles (d) α-crystal size distribution at 2 h.

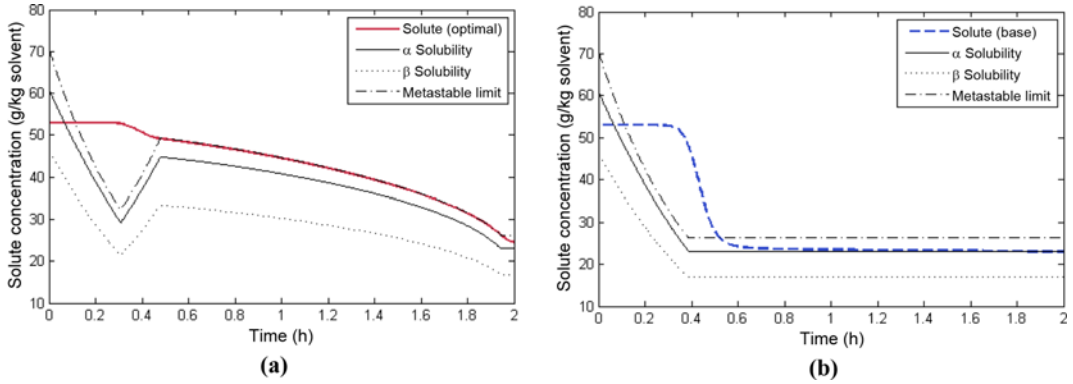

Fig. 6. Solute, saturation, and metastable concentration profiles (a) optimal case (b) base case.

initial cooling, heating, and final cooling steps (Fig. 5(a)). Optimal temperature profile inhibits production of undesired β-form crystals (Fig. 5(b)). From Fig. 5(c) and Fig. 6, the solute concentration remains above metastable limit for shorter time in optimal case than that of base case. The solute concentration returns to the metastable zone from labile region at about 0.48 and 0.52 hours in optimal case and base case, respectively. In Fig. 6(a) and Fig. 6(b), the solute concentration of the optimal case was always close to the metastable limit when it was in the metastable region, while the solute concentration of the base case was near solubility of α-form in the metastable region. In other words, the degree of supersaturation for the optimal case was higher than that of the base case when the operating condition was in the metastable region. Since the growth rate of crystal is increased as the degree of supersaturation is increased, larger crystals could grow in the optimal case. The optimal cooling strategy results in much improved cumulative crystal size distribution of α-crystals (Fig. 5(d)). The cumulative particle number density curve is shifted to the right (larger size) and the slope of the curve becomes much sharper (narrow distribution) in optimal case. The α-crystals with size less than 70 μm are barely produced in the optimal case.

CONCLUSION

Using the equations for nucleation, crystal growth and dissolution rates, and population balance in literature, the crystallization and solvent-mediated polymorphic transformation of LGA was modeled. Metastable limit of LGA was considered in the model and the population balance was solved by using algebraic approximation suggested by Hu et al. Through case study, the cooling-heating-cooling strategy for α-LGA production was suggested and optimal heating onset temperature and heating rate was obtained. The resulting

optimal temperature profile exhibits short nucleation in unstable supersaturated region and long growth period in metastable zone so that large and narrowly distributed α-crystals can be produced. In short, the two cooling periods of the optimized temperature profile can play important roles of seeding and supersaturation control without seed and concentration control. This optimal profile can be an enhanced selective production method of α-LGA. An experimental study is underway to verify this result.

ACKNOWLEDGEMENTS

This work was supported by the Human Resources Development program (No. 20114010203070) of the Korea Institute of Energy Technology Evaluation and Planning (KETEP) grant funded by the Korea government Ministry of Trade, Industry and Energy.

NOMENCLATURE

$a_{\alpha 1}$: first coefficient in solubility of α-form [K^{-2} g (kg solvent)$^{-1}$]
$a_{\alpha 2}$: second coefficient in solubility of α-form [K^{-1} g (kg solvent)$^{-1}$]
$a_{\alpha 3}$: third coefficient in solubility of α-form [g (kg solvent)$^{-1}$]
$a_{\beta 1}$: first coefficient in solubility of β-form [K^{-2} g (kg solvent)$^{-1}$]
$a_{\beta 2}$: second coefficient in solubility of β-form [K^{-1} g (kg solvent)$^{-1}$]
$a_{\beta 3}$: third coefficient in solubility of β-form [g (kg solvent)$^{-1}$]
B_α : nucleation rate of α-form [# m^{-3} s^{-1}]
B_β : nucleation rate of β-form [# m^{-3} s^{-1}]
C : solute concentration [g/kg solvent]
C^*_α : saturated solute concentration (solubility) of α-form [g (kg solvent)$^{-1}$]
C^*_β : saturated solute concentration (solubility) of β-form [g (kg solvent)$^{-1}$]
c_α : solid concentration of α-form [g (kg solvent)$^{-1}$]
c_β : solid concentration of β-form [g (kg solvent)$^{-1}$]
C_{met} : metastable limit of solute concentration [g (kg solvent)$^{-1}$]
D : diffusivity [m^2 s^{-1}]
D_α : dissolution rate of α-form [m s^{-1}]
G_α : growth rate of α-form [m s^{-1}]
G_β : growth rate of β-form [m s^{-1}]
i : index for characteristic length of crystal [-]
J : objective function [-]
$K_{g\alpha}$: exponential factor in the growth rate of α-form [-]
$K_{g\beta}$: exponential factor in the growth rate of β-form [-]
$K_{n\alpha}$: exponential factor in the nucleation rate of α-form [-]
$K_{n\beta}$: exponential factor in the nucleation rate of β-form [-]
$k_{a\alpha}$: surface shape factor of α-form crystal [-]
$k_{a\beta}$: surface shape factor of β-form crystal [-]
$k_{d\alpha}$: mass transfer coefficient in the dissolution rate of α-form [m s^{-1}]
$k_{g\alpha}$: preexponential factor in the growth rate of α-form [m s^{-1}]
$k_{g\beta}$: preexponential factor in the growth rate of β-form [m s^{-1}]
$k_{n\alpha}$: preexponential factor in the nucleation rate of α-form [# m^{-3} s^{-1}]
$k_{n\beta}$: preexponential factor in the nucleation rate of β-form [# m^{-3} s^{-1}]
$k_{s\beta}$: preexponential factor in the β surface nucleation rate [-]
L_α : characteristic length of α-form [m]
$\overline{L}_\alpha$: mean size of α-form crystals [m]
l : normalized size of α-form crystal [-]
$m_{2\alpha}$: 2nd moment of the α particle size distribution [m^2 m^{-3}]
n_α : number density of α-form [# m^{-4}]
r : temperature changing rate [K/min]
S_α : supersaturation for α-form [-]
S_β : supersaturation for β-form [-]
Sc : Schmidt number [-]
T : temperature [K]
T_c : temperature at which initial cooling ends [K]
t : time [s]
w_1 : weighting factor of yield [-]
w_2 : weighting factor of purity [-]
w_3 : weighting factor of crystal size [-]
w_4 : weighting factor of standard deviation [-]
x_α : purity of α-form [-]
Y_α : yield of α-form [-]
z_0 : the first coefficient in metastable limit [g (kg solvent)$^{-1}$]
z_1 : the second coefficient in metastable limit [K^{-1}]

Greek Letters

$\bar{\varepsilon}$: average power input [W kg^{-1}]
ν : kinematic viscosity [m^2 s^{-1}]
ρ_α : solid density of α-form crystal [kg m^{-3}]
ρ_β : solid density of β-form crystal [kg m^{-3}]
σ : normalized standard deviation of α-form crystals [m]
σ_α : standard deviation of α-form crystals [m]

REFERENCES

1. S. Dharmayat, R. B. Hammond, X. Lai, C. Ma, E. Purba, K. J. Roberts, Z.-P. Chen, E. Martin, J. Morris and R. Bytheway, *Cryst. Growth Des.*, **8**(7), 2205 (2008).
2. K. Srinivasan, *J. Cryst. Growth*, **311**, 156 (2008).
3. M. A. O'Mahony, A. Maher, D. M. Croker, Å. C. Rasmuson and B. K. Hodnett, *Cryst. Growth Des.*, **12**(4), 1925 (2012).
4. K. Sypek, I. S. Burns, A. J. Florence and J. Sefcik, *Cryst. Growth Des.*, **12**(10), 4821 (2012).
5. J. Calderon De Anda, X. Z. Wang, X. Lai and K. J. Roberts, *J. Process Contr.*, **15**(7), 785 (2005).
6. N. Garti and H. Zour, *J. Cryst. Growth*, 172, 486 (1997).
7. M. Kitamura, *J. Cryst. Growth*, 96, 541 (1989).
8. C. Cashell, D. Corcoran and B. K. Hodnett, *Chem. Commun.*, **3**, 374 (2003).
9. C. P. Mark Roelands, J. H. ter Horst, H. J. M. Kramer and P. J. Jansens, *AIChE J.*, 53(2), 354 (2007).
10. J. Cornel, C. Lindenberg and M. Mazzotti, *Cryst. Growth Des.*, **9**(1), 243 (2009).
11. H. Hatakka, H. Alatalo, M. Louhi-Kultanen, I. Lassila and E. Hæggström, *Chem. Eng. Technol.*, **33**(5), 751 (2010).
12. Y. Mo, L. Dang and H. Wei, *Fluid Phase Equilib.*, **300**, 105 (2011).
13. J. Calderon De Anda, X. Z. Wang, X. Lai, K. J. Roberts, K. H. Jennings, M. J. Wilkinson, D. Watson and D. Roberts, *AIChE J.*, **51**(5), 1406 (2005).
14. N. C. S. Kee, R. B. H. Tan and R. D. Braatz, *Cryst. Growth Des.*, **9**(7), 3044 (2009).
15. D. R. Yang, K. S. Lee, J. S. Lee, S. G. Kim, D. H. Kim and Y. K. Bang, *Ind. Eng. Chem. Res.*, **46**, 8158 (2007).

16. D. Y. Kim, M. Paul, J.-U. Repke, G. Wozny and D. R. Yang, *Korean J. Chem. Eng.*, **26**(5), 1220 (2009).
17. J. Worlitschek and M. Mazzotti, *Cryst. Growth Des.*, **4**(5), 891 (2004).
18. F. Czapla, H. Haida, M. P. Elsner, H. Lorenz and A. Seidel-Morgenstern, *Chem. Eng. Sci.*, **64**, 753 (2009).
19. J. J. Liu, C. Y. Ma, Y. D. Hu and X. Z. Wang, *Chem. Eng. Res. Des.*, **88**, 437 (2010).
20. C. Y. Ma, X. Z. Wang and K. J. Roberts, *Adv. Powder Technol.*, **18**(6), 707 (2007).
21. C. Y. Ma and X. Z. Wang, *Chem. Eng. Sci.*, **70**, 22 (2012).
22. S. Kumar and D. Ramkrishna, *Chem. Eng. Sci.*, **51**(8), 1333 (1996).
23. S. Kumar and D. Ramkrishna, *Chem. Eng. Sci.*, **52**(24), 4659 (1997).
24. A. Gerstlauer, A. Mitrovic, S. Motz and E.-D. Gilles, *Chem. Eng. Sci.*, **56**, 2553 (2001).
25. B. J. McCoy, *J. Colloid Interface Sci.*, **240**, 139 (2001).
26. B. J. McCoy, *Chem. Eng. Sci.*, **57**, 2279 (2002).
27. G. Madras and B. J. McCoy, *Powder Technol.*, **143-144**, 297 (2004).
28. F. Puel, G. Févotte and J. P. Klein, *Chem. Eng. Sci.*, **58**, 3715 (2003).
29. F. Puel, G. Févotte and J. P. Klein, *Chem. Eng. Sci.*, **58**, 3729 (2003).
30. R. Gunawan, I. Fusman and R. D. Braatz, *AIChE J.*, **50**, 2738 (2004).
31. Q. Hu, S. Rohani, D. X. Wang and A. Jutan, *AIChE J.*, **50**(8), 1786 (2004).
32. Q. Hu, S. Rohani and A. Jutan, *AIChE J.*, **51**(11), 3000 (2005).
33. F. Févotte and G. Févotte, *Chem. Eng. Sci.*, **65**, 3191 (2010).
34. L. F. L. R. Silva, R. C. Rodrigues, J. F. Mitre and P. L. C. Lage, *Comput. Chem. Eng.*, **34**, 286 (2010).
35. N. A. F. A. Samad, R. Singh, G. Sin, K. V. Gernaey and R. Gani, *Comput. Chem. Eng.*, **35**, 828 (2011).
36. J. Schöll, D. Bonalumi, L. Vicum, M. Mazzotti and M. Müller, *Cryst. Growth Des.*, **6**(4), 881 (2006).
37. M. W. Hermanto, N. C. Kee, R. B. H. Tan and M.-S. Chiu, *AIChE J.*, **54**(12), 3248 (2008).
38. S. Qamar, S. Noor and A. Seidel-Morgenstern, *Ind. Eng. Chem. Res.*, **49**, 4940 (2010).
39. Z. K. Nagy, E. Aamir and C. D. Rielly, *Cryst. Growth Des.*, **11**, 2205 (2011).